ORIGINAL ARTICLE

Exploring the effectiveness of negative and positive inserts in machining Inconel 718 alloy: a comparative study

Łukasz Żyłka[1] · Marcin Płodzień[1] · Krzysztof Krupa[2] · Luis Norberto López de Lacalle[3] · Asier Fernandez[3]

Abstract

Inconel 718 alloy is characterised by high strength and corrosion resistance and remains stable at high temperatures, so it is widely used in the energy and aerospace industries. However, machining this material is difficult due to its high strength, hardness, and high specific force coefficient exceeding 3000 MPa. Turning of the Inconel 718 alloy can be carried out with negative and positive inserts. Therefore, the impacts of the insert geometry on the turning process of Inconel 718, cutting force components, and surface roughness were studied. Three positive and three negative insert geometries were tested. It was shown that the key influence on the active components of the cutting force is the effective rake angle. The surface roughness, on the other hand, depends mainly on the cutting-edge radius. It has been shown that the negative insert geometry with $\gamma = 6°$ and $r_n = 22$ μm provides a 30% lower cutting force than the positive inserts and the same surface roughness. The developed models of the cutting force components proved that when cutting with positive inserts, a higher specific cutting force occurs for the Inconel 718 alloy than for the negative insert. It was shown that technological parameters had a very similar effect on the cutting force components and surface roughness parameters regardless of the blade geometry. It was proven that the use of positive inserts makes sense only for depths of cut no greater than the size of the corner radius.

Keywords Inconel 718 · Turning · Tool geometry · Rake angle · Surface roughness · Cutting force

1 Introduction

Inconel alloys, mostly composed of nickel, chromium, and iron, are widely used in the aerospace, automotive, and petrochemical industries due to their exceptional high-temperature strength and corrosion resistance [1]. However, turning Inconel alloys presents substantial machining challenges, which require a thorough understanding of the cutting parameters, the material and geometry of the tools, the cutting conditions, and the cutting forces [2, 3]. The high content of nickel and chromium makes Inconel alloys highly tough and difficult to machine compared to conventional materials [4–6]. Inconel alloys are characterised by high hardness and strength and require robust cutting tools with special geometries and special machining strategies [7]. Obtaining the desired surface quality on Inconel alloys can be challenging due to their hardness [8]. The machining parameters and the selection of tools play crucial roles in determining the final surface quality [9].

Carbide and ceramic cutting tools are commonly used for the machining of Inconel alloys [10, 11]. Ceramic tools typically allow cutting at much higher cutting speeds than

✉ Łukasz Żyłka
   zylka@prz.edu.pl

   Marcin Płodzień
   plodzien@prz.edu.pl

   Krzysztof Krupa
   krupa@prz.edu.pl

   Luis Norberto López de Lacalle
   norberto.lzlacalle@ehu.eus

[1] Department of Manufacturing Techniques and Automation, The Faculty of Mechanical Engineering and Aeronautics, Rzeszow University of Technology, W. Pola 2 Str, Rzeszow 35-959, Poland

[2] Department of Materials Science, The Faculty of Mechanical Engineering and Aeronautics, Rzeszow University of Technology, W. Pola 2 Str, Rzeszow 35-959, Poland

[3] CFAA—Aeronautics Advanced Manufacturing Centre, Biscay Science and Technology Park, University of the Basque Country (UPV/EHU), Ed. 202, Zamudio 48170, Spain

carbide tools and have a much longer tool life. The material removal rate of ceramic tools can even reach 2000% higher than that of carbide tools [11]. However, for economic reasons, the most widely used tool material is carbide. Carbide-cutting inserts used to machine Inconel alloys can have a positive or negative geometry [12, 13]. The advantage of negative inserts is that they can be double-sided and, to achieve a positive relief angle, they must be tilted in the toolholder. This results in a negative rake angle, which increases the strength of the blade but causes an increase in cutting force. Positive cutting inserts, on the other hand, are single-sided, have a positive rake angle as well as a relief angle, and do not need to be inclined in the toolholder. In practice, both types of cutting inserts are used for rough, medium, and finish machining. Furthermore, cutting inserts dedicated to turning nickel alloys can be uncoated or coated with various coatings applied by CVD and PVD techniques [13–17]. However, there is a lack of experimental results on the effect of the type and geometry of the cutting insert on the cutting process of Inconel alloys and the surface quality after turning.

The influence of cutting insert characteristics on the turning process of nickel alloys has been studied in many scientific papers. Paper [12] showed that more compressive stress was generated after cutting with tools with a negative rake angle and a sharp edge radius than after cutting with tools with a positive rake angle and a larger edge radius. The effects of tool geometry on cutting forces and surface roughness were not studied. The effect of the cutting-edge radius of the CBN cutting inserts was also studied in the Inconel 718 turning process. The larger the radius of the edge, the longer the life of the blade; in addition, it was shown that the wear of the insert strongly depends on the depth of the cut [18]. Jemielniak tested eight types of positive and negative turning inserts in the roughing of Inconel 718 [19]. Four types of inserts were used to turn flexible parts and the other types were used to turn rigid parts. The work has shown that the type of insert has a significant influence on the cutting force and stability of the turning process, but its geometry was not determined. A comparison of positive and negative inserts in the turning of Inconel 718 was also carried out in [13]. Zhang et al. tested two negative inserts and one positive insert with different coatings. They measured the wear of the tested tools for different cutting parameters. They showed that negative inserts coated with (Al and Ti) N have a tool life much longer than that of positive and negative inserts coated with TiAlN. It follows that coating has a greater influence on tool life than does its geometry. The influence of the geometry of the tool on the turning of Inconel 718 was the aim of the work [20]. The authors tested four types of inserts that differ in shape and material, but all were negative inserts. The lowest cutting force was recorded at a cutting speed of 250 m/min. Negative inserts

were the subject of most research. For example, Coelho et al. modified the geometry of negative cutting inserts in terms of chamfer length, chamfer angle, and edge radius [21]. The results show that the insert modifications consisting mainly of an increase in the radius of the cutting edge to 13–38 μm caused significant improvements in the insert performance, for example, lower tool wear, temperature, and workpiece surface roughness. Negative inserts with modified edge geometry were also tested in [22]. The modification consisted of making the 0.1 mm-chamfered land at angles of 20° and 30°. The use of modified geometry and cutting edge after honing ensures the induction of compressive residual stresses on the machined surfaces. Fernandez-Valdivielso et al. studied a total of 17 negative insert geometries of the DNMG type. They developed the optimal geometry for turning the Inconel 718 alloy [23]. The 3D topography of the face and the cutting-edge profiles were analysed. The cutting tests revealed that the most effective cutting insert had an effective rake angle of 13° and a cutting-edge radius of approximately 50 μm. However, positive inserts were not tested. The geometry of the cutting inserts in the turning of Inconel alloys has not been the only subject of research. In [24], the authors tested two types of inserts made of two different grades of carbide with cobalt contents of 6% and 10%. A lower Ra roughness parameter was observed for the insert with a 6% cobalt content.

The cutting conditions play an important role in the cutting process of nickel alloys. Therefore, many studies have investigated the effect of cooling conditions on the cutting process of Inconel alloys and the surface quality after turning. Devillez et al. performed semifinishing Inconel 718 turning tests using coated carbide inserts under wet and dry conditions [25]. It was proven that dry machining with a coated carbide tool provides good surface quality, and the residual stresses and microhardness values are the same as those obtained under wet conditions. The role of cooling in Inconel 718 turning was also the subject of research by Raykar [26]. He analysed cutting forces, surface quality, and tool wear under high-pressure coolant conditions, conventional flood cooling, and dry turning. Research shows that a high-pressure coolant and dry turning improve the surface finish. All tests were performed with a single negative type of cutting insert. In addition, in [27], the process of turning Inconel 718 was tested under various conditions. In contrast to other research papers, the results show a higher performance under MQL machining compared to dry and wet conditions.

The cutting parameters have a key influence on the cutting process of nickel alloys and the quality of the workpiece surface. In many scientific papers, the influence of cutting parameters on the turning process and the quality of machined parts has been tested. In [20], the influence of cutting speed and temperature on surface quality was tested.

Research shows that for a tool–workpiece pair in the cutting process, there is an optimal temperature at which the tool–workpiece pair has an optimal strength ratio and the adhesion of the workpiece material is low. In turn, in [21], the influence of feed rate, corner radius, and insert coating methods and materials on surface roughness was tested. It follows from this work that the radius of the insert nose has the most powerful impact on the surface roughness of the workpiece, which is consistent with the relationship for the kinematic surface roughness. The other geometric parameters of the inserts were not tested. The cutting parameters and the radius of the nose of the tool were also the subject of research [28]. Only two negative inserts with different insert corner radii were tested in an Inconel 718 turning process with variable cutting parameters. The analysis showed that the cutting speed and the radius of the nose are the most important parameters that influence the roughness of the surface. On the other hand, the greater the depth of the cut and feed, the greater the surface roughness. It was shown that all cutting parameters had the same influence on the cutting force. The influence of cutting parameters on cutting force, tool wear, and surface roughness was the aim of the work [16]. Research was carried out on the Inconel X750 alloy. The authors proved that the feed has a significant influence on the forces and surface roughness, which is consistent with the results of the work [21, 28]. They also defined the optimal cutting speed for turning Inconel X750, which was equal to 60 m/min. The same alloy was tested in research on the influence of cutting speed and feed on surface roughness [29]. Only negative inserts were used, and it was proven that the feed rate has a greater impact on the surface integrity than the cutting speed. Zębala et al. developed a procedure to optimise cutting data in Inconel 718 turning, the target being maximum cutting efficiency [17]. Surface roughness, cutting force, and cutting temperature were adopted as the limiting criteria. The developed model was tested for only one type of insert that was positive. The analysis clearly shows that the key impact on surface roughness in the turning of nickel-based alloys is the feed rate and corner radius. Other geometric and technological parameters are of secondary importance. Nevertheless, the effects of rake angle, relief angle, entering angle, and cutting-edge radius on surface quality after turning were not analysed.

Modelling the components of the cutting force and the surface roughness parameters during the turning of Inconel 718 has also been the focus of several studies [30–33]. These works have aimed to develop models of force components and primarily the Ra roughness parameter as a function of cutting parameters under various cutting conditions and with different coating inserts. However, it is noteworthy that all the developed models were tailored only to tools with specific geometries. The geometric parameters of the tool were not integrated into the developed models.

Due to the extensive array of geometric variations among the tested tools, coatings, and wide spectrum of cutting parameters investigated, the results obtained in the analysed research exhibit considerable diversity and at times even contradictions. In particular, there are no definitive test results indicating the optimal cutting insert geometry for turning Inconel alloys. Consequently, tool manufacturers offer both positive and negative geometry cutting inserts. Therefore, it is imperative to investigate the disparities between negative and positive geometries when cutting Inconel alloys.

To address this, three negative inserts and three positive inserts, all of which were fabricated from the same coated carbide with a uniform corner radius of 0.4 mm, were meticulously selected for testing. A uniform series of cutting tests was conducted by varying the feed and depth of the cut for each cutting insert. Subsequently, measurements of the cutting force components and surface roughness were meticulously carried out. Then, experimental models were developed for the geometry of the chosen inserts, which included the cutting force components and selected roughness parameters. All the results were analysed, shedding light on the distinctions between negative and positive geometric cutting inserts when machining Inconel alloys.

2 Materials and methods

Experimental cutting process tests were carried out using a test stand constructed around an NEF 600 lathe equipped with a Fanuc 210is control system. The machine tool has a spindle with a maximum rotational speed of 3000 rpm and a maximum power of 24 kW. The maximum possible machining workpiece diameter is 600 mm and workpiece length is 1250 mm. The cutting force components were precisely measured using a Kistler 9257B piezoelectric dynamometer with a measuring range of ± 5 kN. This dynamometer was attached to the turret head of the machine tool via a VDI holder. The signal from the dynamometer was then transmitted to a computer through a 16-bit analogue-to-digital converter NI9215 provided by National Instruments, facilitated by a Kistler type 5070 load amplifier, and connected via USB (see Fig. 1). Signal visualisation, processing, and recording were performed through a program developed within the LabVIEW software environment. The signal sampling frequency was set at 5 kHz.

Turning tests were conducted on a workpiece shaped like a shaft made of INCONEL® alloy 718 (UNS N07718/W.Nr. 2.4668) in the annealed state (34 HRC hardness), measuring 50 mm in diameter and 90 mm in length. Throughout the length of the shaft, nine machining passes were executed using a single tool, each with distinct technological parameters. A consistent cutting speed of 40 m/min was
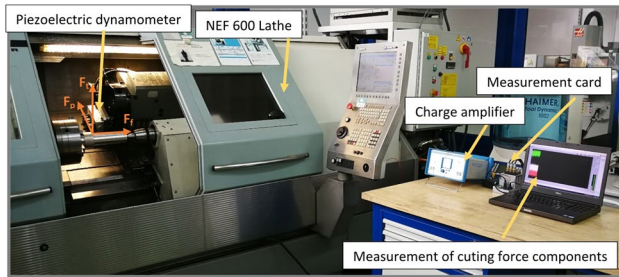
Fig. 1 Test stand

used, which was optimised for the AH8015 carbide. The remaining cutting parameters, feed rate (*f*) and depth of cut (a_p), were varied according to a comprehensive plan. The experimental design followed the principles of the design of experiments (DoE), according to the statistical plan, a central composite fractional design with three levels and two factors. Feed rates were 0.08, 0.1, and 0.12 mm/r, while the cut depth ranged from 0.4 to 1.2 mm. Therefore, nine cutting tests with different cutting parameters and four repetitions were performed for each cutting insert. The selection of the depth-of-cut values was determined by the corner radius (r_ε), ensuring depths corresponding to r_ε, twice r_ε, and thrice r_ε. The cutting depth range was selected to test the operation of the cutting edge within the radius of the corner and along its length. Furthermore, the cutting depth and feed values were selected as recommended by the turning tool manufacturer. The cutting depth and feed values were selected to be within the operating range of chip breakers, i.e. recommended for each insert geometry. The ap and *f* values corresponded to finishing and medium machining and are useful ranges used in Inconel turning. In addition, the values of the technological parameters were chosen to align with the conditions of other tests [13, 14].

2.1 The geometry of the cutting tools

Six Tungaloy-made cutting inserts, specifically designed to turn Inconel alloys, were tested. Among these, three were double-sided negative-type VNMG inserts, while the remaining three were single-sided positive-type VBMT inserts. All inserts utilised were 160,404 in size and were constructed from AH8015 grade (ISO S10), which consists of a sintered carbide (submicro-grain of approximately 10% Co) nanostructured multilayer PVD coating with a high aluminium content (refer to Fig. 2). Turning tools with PVD coatings are very often used for turning nickel-based alloys [13, 15, 16, 34].

Dry conditions were used to eliminate the influence of the type of coolant and the conditions of its supply to the cutting zone on the cutting force and surface roughness. Machining passes were performed only on a shaft length of 10 mm.
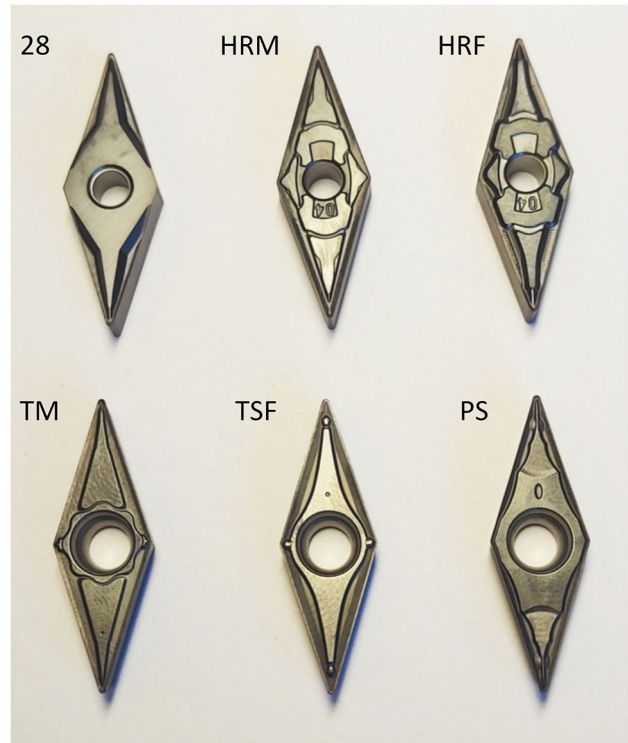

Fig. 2 Types of geometries tested

For a minimum feed rate of 0.08 mm/rev, the spiral cutting length (SCL) did not exceed 20 m. With such a short turning length, the wear of the blade, even under dry machining conditions, is not noticeable and does not affect the test results [34]. However, the tool wear (*VB*) of each cutting insert was controlled and its value was always less than 0.1 mm.

The negative inserts featured three distinct geometries, each serving a specific purpose:

- 28—medium machining
- HRM—finishing, medium cutting, and roughing
- HRF—finishing

On the other hand, positive inserts were characterised by the following geometries:

- TM—medium machining
- TSF—finishing
- PS—finishing and medium machining

Given the diverse range of geometries among the tested cutting inserts and the distinct positioning of the negative inserts within the holder compared to the positive inserts (as illustrated in Fig. 3), the blade geometry within the tool system was evaluated after the clamping of inserts in the toolholder. This assessment was performed by scanning the blades using an Alicona Infinite Focus microscope. Figure 4
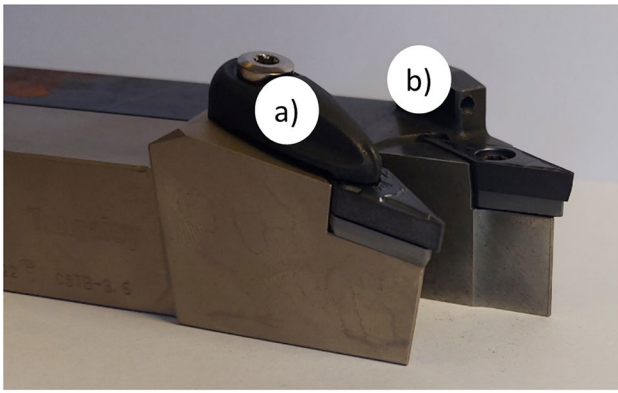
Fig. 3 Positioning of the insert in the holder: **a** negative insert, **b** positive insert

provides a visual representation of the scanned blades, where solid lines indicate the ranges corresponding to the three depths of cut tested, while dashed lines delineate the ranges associated with the three feed rates tested.

Subsequently, the size of the cutting-edge radius (r_n) was determined for each blade, and the values for the back rake angle and the average effective rake angle were calculated with respect to the depth of cut. The back rake angle was precisely defined within the plane of the main cutting edge (refer to Fig. 5).

In the Tables 1, 2, and 3, the values of the geometrical parameters for all the tested cutting inserts are presented.

When analysing the geometry of the tested blades, it becomes evident that they exhibit varying values of the cutting-edge radius. The smallest values are observed for the HRM blade type, which boasts a broad range of applications, and the type 28 blade, which is specifically designed for medium machining. In contrast, the HRF blade features the largest radius, despite being dedicated to finishing operations. In contrast, the disparities in the size of the cutting-edge radius are much less pronounced for positive inserts. Negative inserts are characterised by a notably large negative λ angle, which is achieved by inclining the cutting inserts negatively within the toolholder. Among these, the HRM-type insert displays the largest λ angle. In contrast, in positive inserts, the λ angle is close to zero as a result of the absence of inclination of the insert in the toolholder. For the TM and TSF blades, slight edge inclination is observed only at specific cutting-edge lengths (refer to Table 2).

Determining the rake angle at the tested depths of cut proved to be particularly challenging due to its significant variation in the face (as depicted in Fig. 2). Table 3 presents the average values of the effective rake angles, excluding the rounded area of the cutting edge. However, all tested cutting inserts exhibited highly disparate face geometries. In particular, blade 28 stands out as the sole insert with a negative effective rake angle within the corner radius range

r_ε, fluctuating between $-4°$ and $4°$ across the depth of cut. In contrast, the HRM blade maintains a consistent geometry throughout the depth of cut. Similarly, the TSF blade demonstrates an almost uniform effective rake angle, albeit half that of the HRM blade. In contrast, the HRF blade boasts the highest effective rake angle; for a depth of cut $a_p > 0.4$ mm, the rake angle reaches approximately 14°. The TM and PS blades also feature positive effective rake angles; however, their values exhibit significant fluctuations along the length of the cutting edge. Analysis of the blade geometries under examination facilitated the definition of their fundamental geometrical parameters, which was instrumental in analysing the turning process of the Inconel 718 alloy.

3 Results and discussion

3.1 Cutting force component analysis

The F_t force operates along the direction of the cutting speed vector; it is a tangential force associated with the material separation process. In contrast, the F_f force corresponds to the velocity vector of the feed motion. Both F_t and F_f are active forces directly involved in the cutting process. However, the F_r force, which acts perpendicular to the surface of the workpiece, is a passive force that is not related to any movement. Its role is to induce repulsion of the workpiece from the tool, thereby influencing the dimensionality and shape accuracy of the workpiece.

Given the distinct roles of each force component, comprehensive measurements and analyses of all three cutting force components were carried out. Additionally, the resultant value of the cutting force was determined. The results of the recorded cutting force components and the resultant force values are presented as a function of the feed rate (Figs. 6, 7, 8 and 9). The feed influences the cross section of the cut layer and is related to the specific cutting force factor K_c.

The value of the F_f feed force component undergoes significant changes with variations in feed f and the depth of cut a_p (Fig. 6). These changes are not only attributed to alterations in the cross-sectional area of the cut layer but also influenced by variations in tool geometry along the length of the cutting edge of certain insert types. In particular, the feed rate predominantly influences the force, while the depth of cut also impacts the intensity of the force variation, a phenomenon that differs between different insert geometries. The dominant influence of feed rate on the F_f force is also confirmed by the results of other works [21]. Consequently, different insert geometries achieve the lowest and highest force values at varying depths of cut (Fig. 6).

When employing a depth of cut equivalent to the corner radius r_ε, the HRF negative and PS positive geometries exhibited the lowest feed force F_f (Fig. 6a). Within the $a_p =$
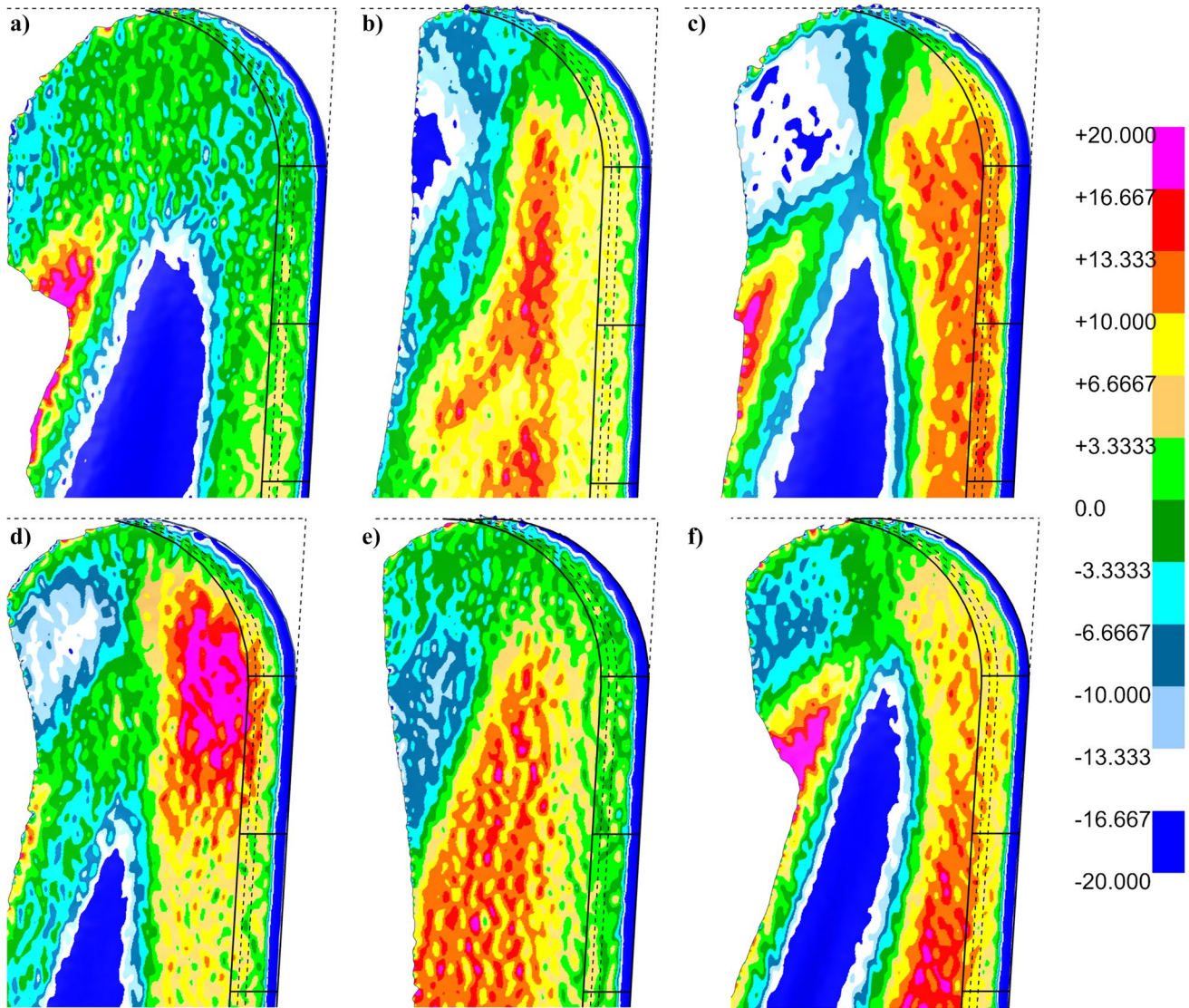
Fig. 4 Face geometry of the following inserts: **a** 28, **b** HRM, **c** HRF, **d** TM, **e** TSF, and **f** PS

0.4 mm range, these geometries feature positive effective rake angles of 10° and 6°, respectively. Despite their relatively large cutting-edge radius values, these geometries yielded the lowest feed forces, indicating the dominant influence of the effective rake angle. Conversely, geometry 28, characterised by a negative effective rake angle despite

Fig. 5 The view of the HRF blade in the main cutting-edge plain

having the smallest cutting-edge radius r_n, yielded the highest values of the F_f component.

With a deeper a_p equal to twice the corner radius r_ε, the HRM geometry yielded the lowest values of the F_f component (Fig. 6b, c). This outcome can be attributed to the increased significance of the radius r_n of the cutting edge when engaging the cutting edge on a longer length. Thus, a combination of a small radius (r_n) and a positive effective rake angle proves to be most advantageous in this scenario. These findings are corroborated by the results obtained at the greatest depth of cut (a_p= 1.2 mm), where the HRM geometry consistently generated the lowest F_f force values. This outcome is possibly due to the positive and consistent effective rake angle throughout the length of the edge, along with the small radius of the rounded cutting edge r_n. Additionally,
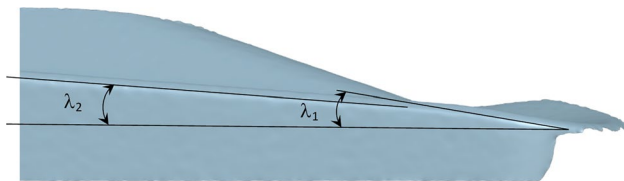
Table 1 Values of the cutting-edge radius

Insert number	Type of insert geometry	Cutting-edge radius, r_n (µm)
1	28	20
2	HRM	22
3	HRF	32
4	TM	28
5	TSF	25
6	PS	27

the considerable negative back rake angle observed in the HRM geometry contributes to this favourable performance.

In contrast, geometry 28 exhibited the highest F_f force values, with differences of up to 70% compared to those of the HRM. However, very similar F_f force values were observed for the other geometries at the greatest depths of cut.

The analysis unmistakably demonstrated that both the cutting-edge radius and the effective rake angle play pivotal roles in determining the F_f component. The optimal results, characterised by the lowest forces, were achieved through a combination of the smallest cutting-edge radius r_n and a positive effective rake angle, maintaining a constant value throughout the cutting-edge length. Notably, the lowest F_f force values were attained for both negative and positive inserts, irrespective of their blade geometry, underscoring the nuanced interplay of these factors in force generation.

The analysis of the tangential force F_t yields conclusions similar to those drawn from the analysis of the force F_f (Fig. 7). When cutting with a corner radius, i.e. with a depth of 0.4 mm, the HRF and PS geometries exhibited the lowest F_t forces, while geometry 28 and the TSF yielded the highest forces. Upon increasing the depth of cut to 0.8 mm, almost all the geometries produced very similar F_t force values, except for geometry 28, which generated forces approximately 20% greater than those of the other geometries (Fig. 7b). For the largest depth of cut, the HRM geometry, characterised by a small radius of the rounded cutting edge and a constant positive effective rake angle,

Table 2 Values of the back rake angle for the tested geometries

a_p, mm	Back rake angle λ, °					
	28	HRM	HRF	TM	TSF	PS
0.4	− 4	− 13	− 8	0	− 2	0
0.8	− 4	− 13	− 4	6	0	0
1.2	− 4	− 13	− 4	0	0	0

Table 3 Values of the effective rake angle for the tested geometries

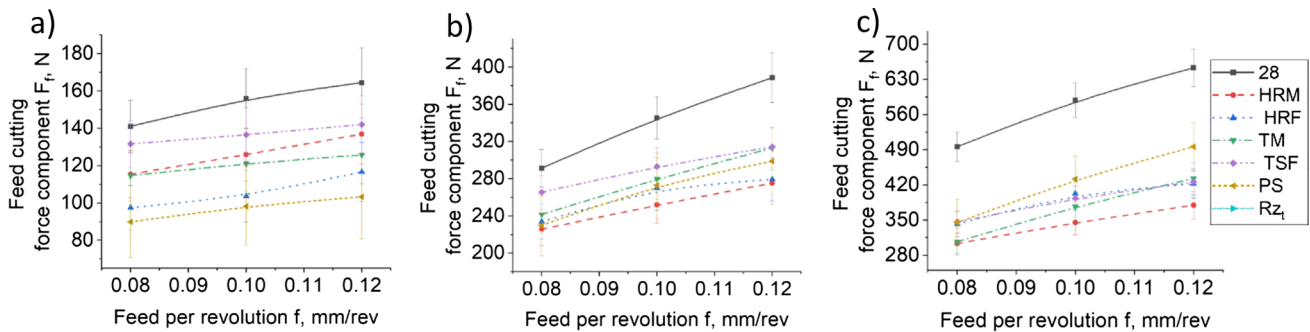| a_p, mm	Effective rake angle γ, °					
	28	HRM	HRF	TM	TSF	PS
0.4	− 4	6	10	3	0	6
0.8	0	6	14	13	3	10
1.2	4	6	14	6	3	10

Fig. 6 Feed force component F_f for different cutting depths: **a** 0.4 mm, **b** 0.8 mm, and **c** 1.2 mm
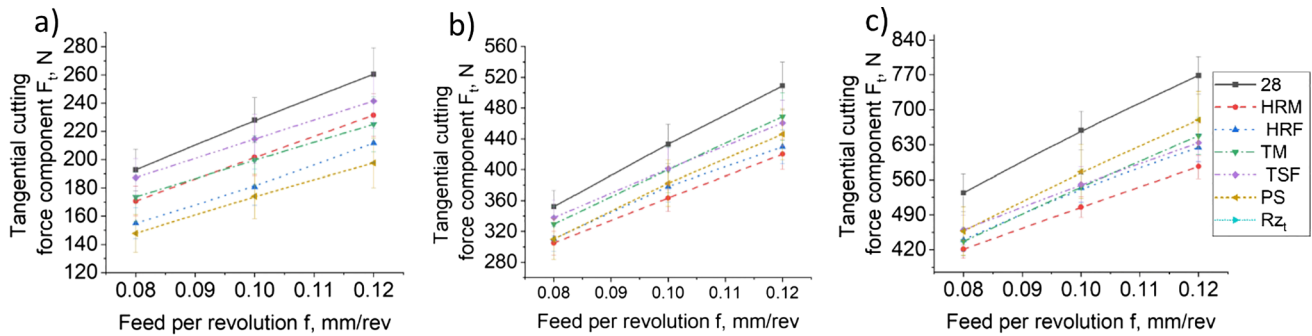
Fig. 7 Tangential force component F_t for different cutting depths: **a** 0.4 mm, **b** 0.8 mm, and **c** 1.2 mm

generated the lowest F_t force value, with geometry 28 producing a force approximately 30% greater (Fig. 7c).

Furthermore, it is noteworthy that the HRM geometry exhibited the smallest dispersion of values, indicative of the greatest stability in the cutting process. Positive inserts, on the other hand, displayed an F_t force approximately 10% greater than that of the HRM geometry.

As the depth of cut a_p increases, the discrepancies in the values of the F_t and F_f forces between the inserts become more pronounced, primarily due to variations in the blade geometry. Geometry 28, for example, exhibits a fluctuation in the effective rake angle along the length of the cutting edge, ranging from -4 to $+4°$. Within the corner radius range, the effective rake angle is negative, transitioning to positive values, although reaching a maximum of only 4° at a cutting depth of 1.2 mm. This particular geometry tends to generate high forces F_t and F_f.

In contrast, the HRM geometry consistently generates the lowest active forces. This can be attributed to the small value of the cutting-edge radius and the constant positive effective rake angle. Additionally, the HRM geometry maintains a constant and strongly negative back rake angle. For shallower depths of cut, the differences between geometries are relatively minor and fall within the spread of force values.

Analysis of the radial force F_r leads to markedly different conclusions (Fig. 8). First, it is important to note that the values of the F_r force are approximately three to four times smaller than those of the active components of the cutting forces F_t and F_f, indicating that Fr has relatively less significance. Additionally, there is a minor influence of technological parameters on the value of the F_r force component. Throughout the entire range of cutting depths and feed rates examined, the F_r force values ranged from 100 to 200 N, while the F_t force values ranged from 150 to 770 N.

Upon analysis of the graphs in Fig. 8, it becomes evident that the HRM geometry generates the highest value of the radial force F_r. However, even at the maximum technological parameters, its value does not exceed 200 N, accounting for only 30% of the F_t force. Conversely, the TM and PS

geometries exhibited the lowest F_r force. Further examination of the blade geometry underscores the predominant role of the back rake angle. The TM and PS geometries stand out as the only ones characterised by a positive or zero λ angle, while the HRM geometry boasts a strongly negative λ angle of up to $-13°$.

In general, positive inserts tend to generate lower F_r force values. This confirms the results obtained in the papers [19, 21]. However, the difference between the forces generated by positive and negative inserts often falls within a dispersion of its values. In particular, these differences became more noticeable and significant only for higher feed rates and at greater cutting depths. Hence, cutting inserts with positive geometries can be dedicated to turning flexible workpieces [19].

Due to the varying variability of active and passive forces across different geometries, an analysis of the resultant force F values was conducted (Fig. 9). At the highest depth of cut and for all feeds, geometry 28 yielded a force approximately 45% greater than that of the HRM geometry. In contrast, the HRM geometry exhibited a force approximately 10% lower than that of the other geometries. For a depth of cut of 0.8 mm, the differences were smaller, with geometry 28 still generating the highest force, approximately 25% greater than that of the other inserts. However, the HRM geometry provided the lowest force, and the difference between the HRM geometry and the other geometries was only a few percent.

In contrast, for the smallest depth of cut, the PS geometry produced the lowest total force. In particular, the analysis of the total force F aligns with the analysis of the changes in the forces F_t and F_f, confirming the negligible effect of the force F_r on the overall load and energy of the cutting process.

The analysis revealed that the utilisation of positive inserts is only advantageous for cutting at small depths, closely approaching the size of the corner radius. In such scenarios, a reduction in force of up to 30% can be achieved by employing positive inserts, especially the PS geometry (Fig. 9a). However, as the engagement of the cutting edge increases, particularly at depths of cut that exceed the radius
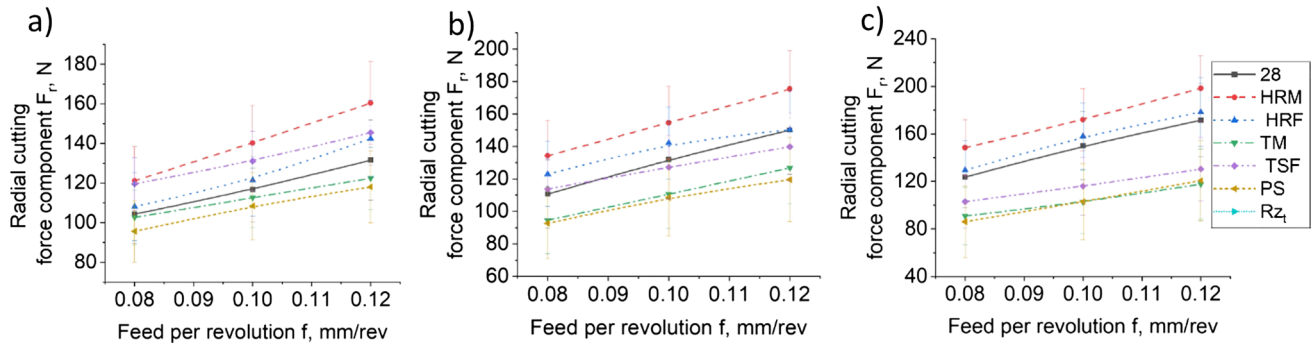
Fig. 8 Radial force component F_r for different cutting depths: **a** 0.4 mm, **b** 0.8 mm, and **c** 1.2 mm

of the corner, the geometry of the blade assumes greater significance.

The lowest forces were observed for negative inserts featuring a constant positive effective rake angle, along with a consistent and strongly negative back rake angle, coupled with a small edge radius of approximately 0.02 mm. Consequently, these analyses show that for cutting depths exceeding the corner radius, negative inserts with HRM-type geometries are preferable. Negative inserts characterised by variable rake angles, such as geometry 28, should be avoided in such applications.

Because it has been demonstrated that the effective rake angle γ has a dominant influence on the cutting force F, the cutting force was analysed as a function of the effective rake angle for both positive and negative cutting inserts. The results are presented in Fig. 10 for the maximum feed rate of 0.12 mm/rev and for three different cutting depths, as the effective rake angle depends on the a_p parameter (Fig. 4).

At most cutting depths, as the effective rake angle of the negative inserts increased, the cutting force F decreased. However, for the largest depth of cut (a_p= 1.2 mm), different dependencies were observed. This is because the greater the cutting depth is, the greater the length of the cutting edge working in the material. Therefore, the radius of the cutting edge r_n plays a more significant role. Consequently, the forces recorded for the effective rake angle of 14° are greater than those for $\gamma = 6°$ because the blade with $\gamma = 14°$ has a cutting-edge radius r_n greater by 0.01 mm compared to the other inserts (Fig. 10a). It can be seen that the lowest cutting force F, especially for the two largest cutting depths, was recorded for an effective rake angle of 6°, that is, for the HRM geometry. From this analysis, it is evident that the optimal value of the effective rake angle for the negative insert is 6°; a further increase does not reduce the cutting force.

Analysis of the cutting force F for positive inserts yielded similar conclusions. In the range of the lowest cutting depth, that is, within the corner radius r_ε, the effective rake angle γ plays a significant role, and with an increase in the γ angle, the force F decreases. For greater cutting depths, a lower and more irregular influence of the effective rake angle can be observed. It is not possible to select a positive geometry that generates the lowest cutting force for the entire range of parameters tested. By analysing the curves in Fig. 10b, it can be inferred that, similar to negative inserts, the lowest cutting forces should be achieved throughout the range of cutting depths for an effective rake angle of 6°. However, even assuming the optimal rake angle for both negative and positive inserts ($\gamma = 6°$), lower forces are still generated by
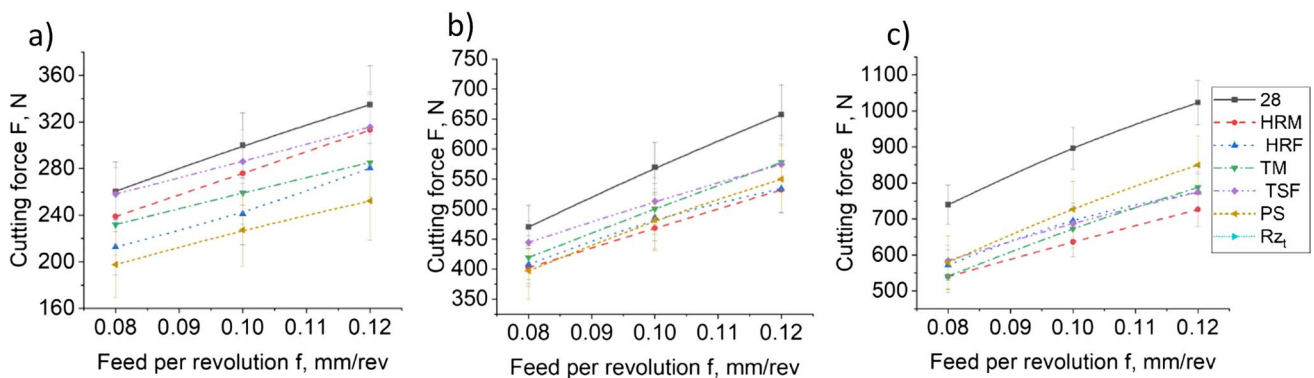

Fig. 9 Resultant cutting force for different cutting depths: **a** 0.4 mm, **b** 0.8 mm, and **c** 1.2 mm
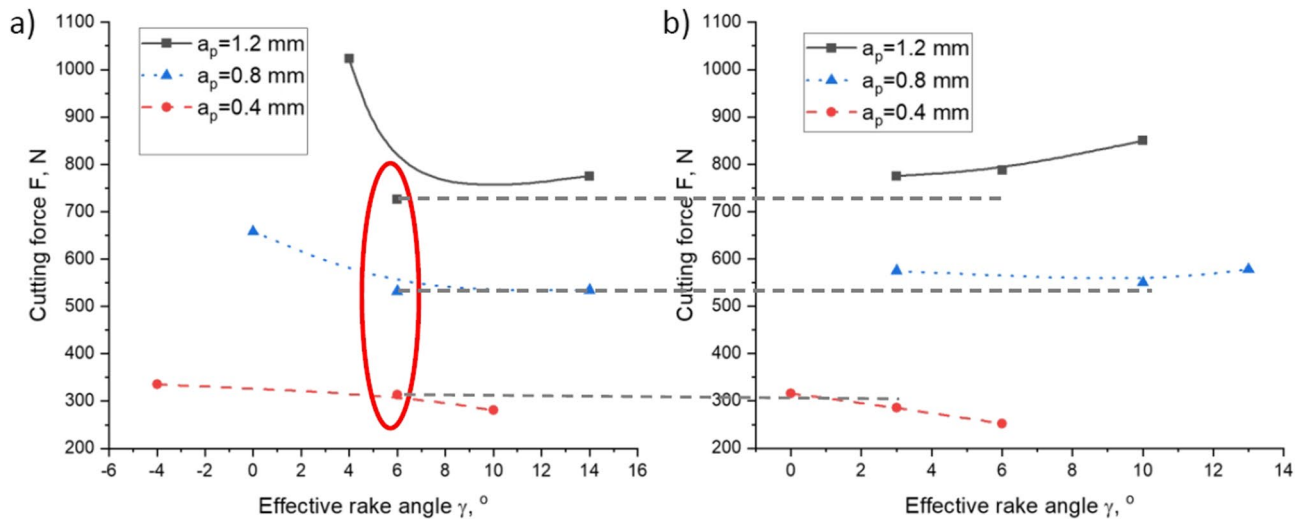
Fig. 10 Changes in the resultant cutting force as a function of the effective rake angle for **a** negative inserts and **b** positive inserts

the negative inserts. This is presumably because negative inserts have a negative back rake angle λ, which beneficially affects the cutting process by deflecting chips away from the edge and reducing the cutting force F.

Taking into account the aforementioned analysis, one HRM negative geometry and one PS positive geometry were chosen. The HRM geometry exhibited the lowest cutting forces among the negative inserts, while the PS geometry demonstrated the lowest cutting forces among the positive inserts across most cutting parameters, especially for the lowest depth of cut. Hence, these optimal geometries were compared in terms of cutting forces.

Experimental models were developed for each component of the cutting force for both geometries and subsequently compared. Table 4 presents the models obtained along with their statistical parameters, while Fig. 11 offers a graphical interpretation of these models.

Upon analysing the models of the cutting force components, it becomes apparent that there are slight differences in the formulas between the negative and positive inserts. For the HRM negative insert, predominantly linear models were obtained, with only the F_t component having a two-way interaction factor. These models demonstrate a very good fit of more than 90%. However, a small fitting error is present in each model, which is not observed in the force component models for the positive insert.

In contrast, all models for the PS positive insert feature a two-way interaction component. Additionally, the F_t force model includes a quadratic component, although its P-value increases, indicating less statistical significance. Furthermore, its contribution to the model is negligible, as evidenced by the quasiflat curvature of the function in Fig. 11b. However, in the F_t force model for the positive

insert, the contribution of nonlinear components exceeds that in the model for the negative insert.

Significant differences are observed in the models of the force component F_r, attributable to variations in the values of the back rake angle. Consequently, in the positive insert model, the contribution of feed f exceeds 94%, signifying that the radial component F_r depends solely on the feed rate. However, in the case of negative geometry, the force F_r is additionally influenced by the depth of cut, with its contribution to the model exceeding 15%. This can be attributed to the negative back rake angle in the direction of the depth of cut.

Furthermore, the F_f component is more dependent on the depth of cut than on the feed rate, as confirmed by the results in Fig. 11e and f. An increase in the depth of cut leads to a significantly more pronounced increase in the force F_f than to an increase in the feed rate f. The influence of the feed rate is slightly stronger for the PS positive geometry. Additionally, a two-way interaction component is present in the model for the PS positive insert, which causes an additional feed contribution.

Previous research work has mainly developed linear models of cutting force components [30, 32]. However, these models additionally took into account the contribution of either the cutting speed or the corner radius r_ε. However, the conclusions of other works have confirmed that, in the case of the feed force component, the greatest contribution is made by the feed rate. For the other forces, the depth of cut has the greatest contribution [30, 33].

The resulting models of the cutting force components exhibit very similar forms. Each force equation comprises a constant value alongside cutting parameters such as a_p and f, which are multiplied by coefficients. In line with the Kienzle

Table 4 Experimental models of cutting force components

Negative insert VNMG 160,404-HRM					Positive insert VBMT 160,404-PS				
$Ft = 13.3 + 83.6\,a_p + 378\,f + 2988\,a_p f$					$Ft = 43.5 + 32.3\,a_p - 917\,f - 47.0\,a_p^2 + 5400\,a_p f$				
Source	DF	Contr.	F-value	P-value	Source	DF	Contr.	F-value	P-value
Model	3	99.79%	946.87	0.000	Model	4	99.98%	5256.07	0.000
Linear	2	98.18%	1418.80	0.000	Linear	2	97.20%	10,220.02	0.000
a_p	1	84.40%	2665.11	0.000	a_p	1	87.01%	18,297.37	0.000
f	1	13.78%	349.22	0.000	f	1	10.19%	2142.67	0.000
2-way int.	1	1.61%	45.90	0.001	Square	1	0.04%	8.71	0.042
$a_p f$	1	1.61%	45.90	0.001	a_p^2	1	0.04%	8.71	0.042
Error	6	0.21%			2-way int.	1	2.74%	575.54	0.000
Lack-of-fit	5	0.10%	0.18	0.934	$a_p f$	1	2.74%	575.54	0.000
Pure error	1	0.11%			Error	4	0.02%		
Total	9	100.00%			Total	8	100.00%		
$Fr = 6.4 + 34.25\,a_p + 1206\,f$					$Fr = 70.60 - 43.25\,a_p + 393.4\,f + 381.1\,a_p f$				
Source	DF	Contr.	F-value	P-value	Source	DF	Contr.	F-value	P-value
Model	2	93.13%	47.43	0.000	Model	3	99.06%	175.50	0.000
Linear	2	93.13%	47.43	0.000	Linear	2	96.07%	255.31	0.000
a_p	1	15.18%	25.61	0.001	a_p	1	2.03%	10.80	0.022
f	1	77.95%	79.40	0.000	f	1	94.04%	499.82	0.000
Error	7	6.87%			2-way int.	1	2.99%	15.88	0.010
Lack-of-fit	6	3.36%	0.16	0.954	$a_p f$	1	2.99%	15.88	0.010
Pure error	1	3.51%			Error	5	0.94%		
Total	9	100.00%			Total	8	100.00%		
$Ff = -91.7 + 275.8\,a_p + 1122\,f$					$Ff = 85.1 - 20.8\,a_p - 1493\,f + 4295\,a_p f$				
Source	DF	Contr.	F-value	P-value	Source	DF	Contr.	F-value	P-value
Model	2	98.18%	188.65	0.000	Model	3	99.84%	1044.61	0.000
Linear	2	98.18%	188.65	0.000	Linear	2	97.13%	1524.42	0.000
a_p	1	94.14%	375.27	0.000	a_p	1	91.94%	2885.71	0.000
f	1	4.04%	15.52	0.006	f	1	5.20%	163.13	0.000
Error	7	1.82%			2-way int.	1	2.71%	84.99	0.000
Lack-of-fit	6	0.94%	0.18	0.944	$a_p f$	1	2.71%	84.99	0.000
Pure error	1	0.88%			Error	5	0.16%		
Total	9	100.00%			Total	8	100.00%		

and Altintas cutting force equations, the multiplication factors of the product a_p and f can be interpreted as the specific cutting force K_c [35]. Taking this into account, it becomes evident that the multiplier of a_p and f in the two-way factors is notably greater in the active force component models of the cutting force for the positive insert. For instance, in the tangential force model F_t for the negative insert, the multiplier of a_p and f, i.e. the specific cutting force K_c, is equal to 3000, whereas for the positive insert, it is equal to 5400. Additionally, the feed multiplier is more than two times greater in the positive insert model than in the F_t model of the negative insert. Specifically, in the case of the feed component of the cutting force F_f, the feed multiplier f for the positive insert is 40% greater than the feed f multiplier in the force F_f model of the negative insert. Furthermore, in the positive insert F_f model, there is an additional two-way

factor with a multiplication factor of approximately 4300. This indicates that cutting with a positive insert results in a higher specific cutting force for the Inconel 718 alloy (K_c= 4300–5400 MPa), while in the case of a negative insert, the specific cutting force is much lower (K_c= 3000 MPa). Consequently, the cutting resistance of the Inconel 718 alloy is significantly greater for positive inserts than for negative inserts, leading to markedly greater cutting forces when machining Inconel alloys using positive inserts.

From the analysis, it can be inferred that technological parameters exert a very similar effect on the cutting force components for both types of geometry, as evidenced by the graphs in Fig. 10. Notably, for the positive geometry, a much steeper response surface shape was observed for components F_t and F_f. The most substantial difference lies in the models
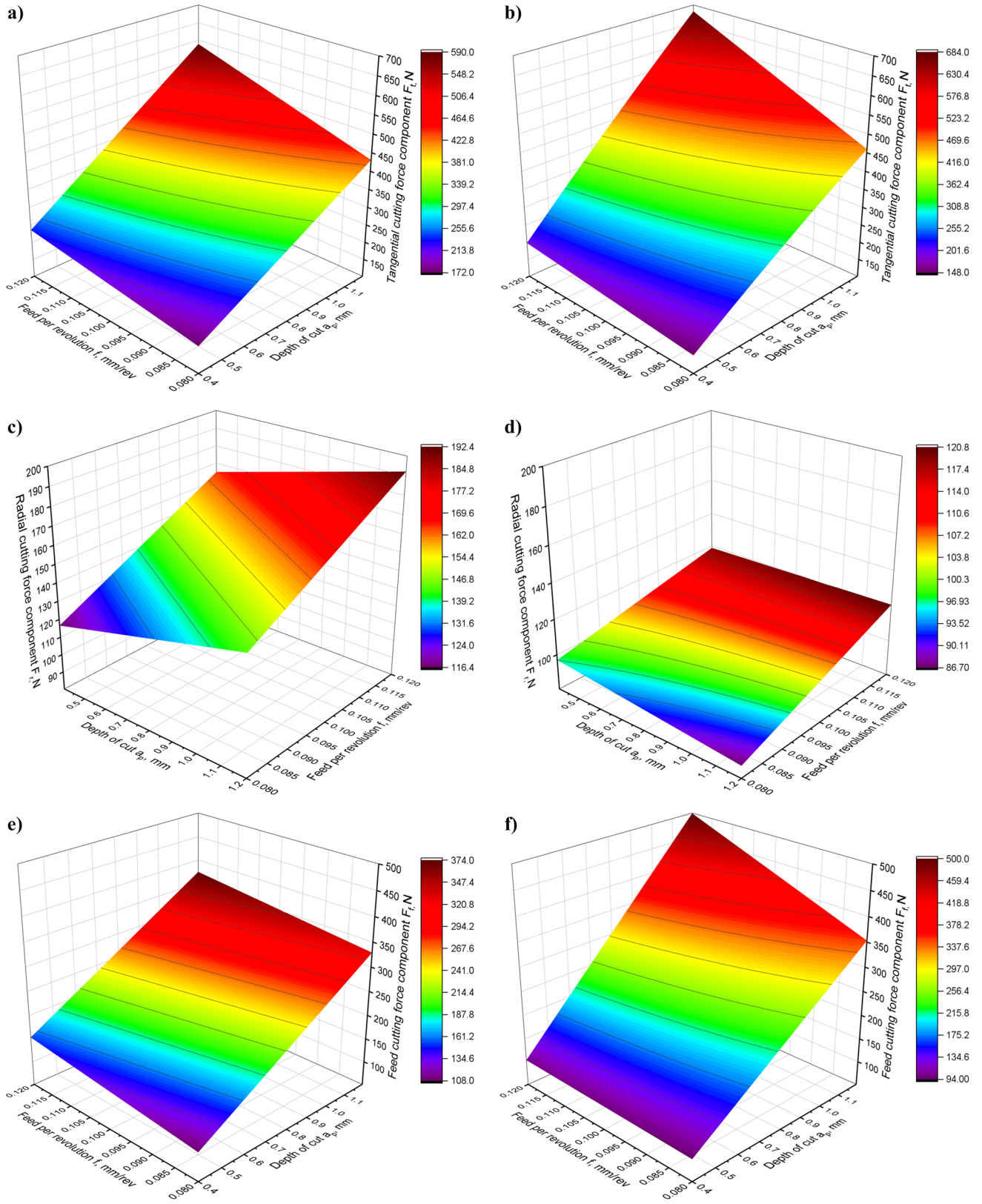
Fig. 11 Graphical representation of the cutting force component models for the HRM geometry **a** F_t, **c** F_r, **e** F_f and PS geometry **b** F_t, **d** F_r, **f** F_f

of the F_r component, which can be attributed to the geometry of the blade, specifically the angle λ.

These findings underscore that technological parameters have a comparable impact on the components of the cutting force, thereby emphasising the pivotal role of blade geometry in determining cutting forces.

3.2 Surface roughness analysis

The surface roughness is a crucial quality parameter of a workpiece. The most commonly used roughness parameters in practice are Ra and Rz. Ra is the average surface roughness and is the integer mean of all absolute roughness profile deviations y from the centerline within the measurement length L_m and is expressed by the following formula:

$$R_a = \frac{1}{L_m} \int_o^{L_m} |y| dx \tag{1}$$

Since Ra represents the average value, Rz is based on the maximum value. Therefore, both parameters are often used simultaneously to describe surface roughness. To calculate Rz, the roughness profile is divided into five equal lengths. The height difference between the highest and lowest points in each of the five sections is the total roughness. In other words, Rz is the average of the five Rt values from Rt_1 to Rt_2. The calculated Rz is approximately equal to the height of the most severe roughness variation and is calculated by the following formula:

$$R_z = \frac{1}{5}\left(R_{t1} + R_{t2} + R_{t3} + R_{t4} + R_{t5}\right) \tag{2}$$

To evaluate the impact of blade geometry on the two fundamental roughness parameters Ra and Rz, variations in the depth of cut and feed rate were studied. The results are depicted in Figs. 12 and 13. To compare the real values of the Ra and Rz parameters with the kinematic roughness of

the surface, the theoretical values of the Ra_t and Rz_t roughness parameters were also calculated according to the relationships [36]:

$$Ra_t = \frac{f^2}{32 r_\epsilon} 1000 \tag{3}$$

$$Rz_t = \frac{f^2}{8 r_\epsilon} 1000 \tag{4}$$

The calculated theoretical values of the Ra_t and Rz_t parameters are presented in Table 5. Also in Figs. 12 and 13, their values are given as a function of the feed to compare them with the measured values of surface roughness parameters.

Upon analysing the graphs in Figs. 12 and 13, it becomes evident that the effect of blade geometry on surface roughness remains consistent across different cutting depths and feed rates. Regardless of the technological parameters, the HRF- and TM-type geometries consistently yield the highest surface roughness. Likewise, the TSF geometry is characterised by an increased surface roughness compared to that of other cutting inserts.

The analysis of the blade geometry suggested that the radius of the cutting edge r_n plays a dominant role in surface roughness. The blades with the highest radius r_n, approximately 0.03 mm, cause the highest roughness of the workpiece surface. In contrast, the TSF geometry, although it has a slightly smaller cutting-edge radius, features a very small effective rake angle, making chip formation more challenging and potentially contributing to deteriorated surface roughness.

Among all geometries tested, the lowest roughness is achieved by two negative geometries and one positive geometry. The PS geometry, characterised by a relatively large radius of the cutting edge, compensates for the large positive effective rake angle and is maintained consistently at 10° along the cutting edge. Moreover, the λ angle remains
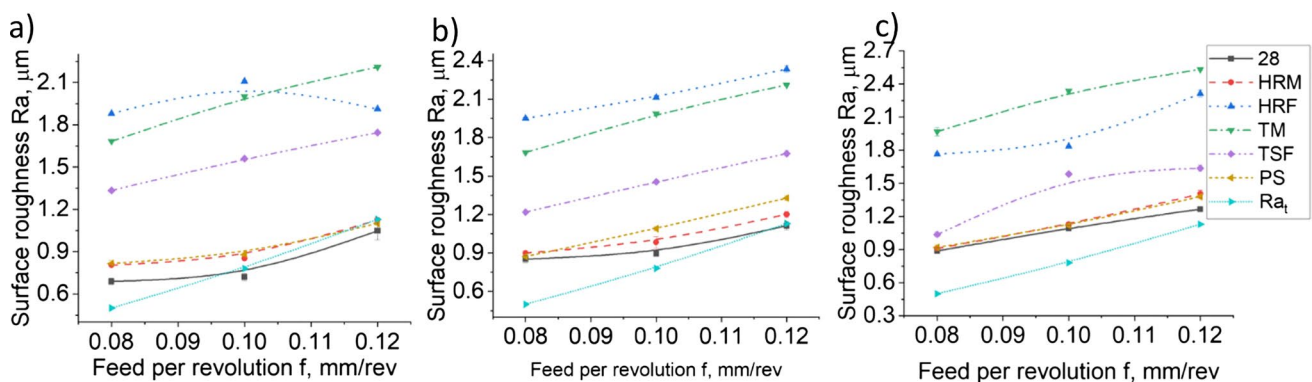

Fig. 12 Surface roughness Ra parameters for different cutting depths: **a** 0.4 mm, **b** 0.8 mm, and **c** 1.2 mm
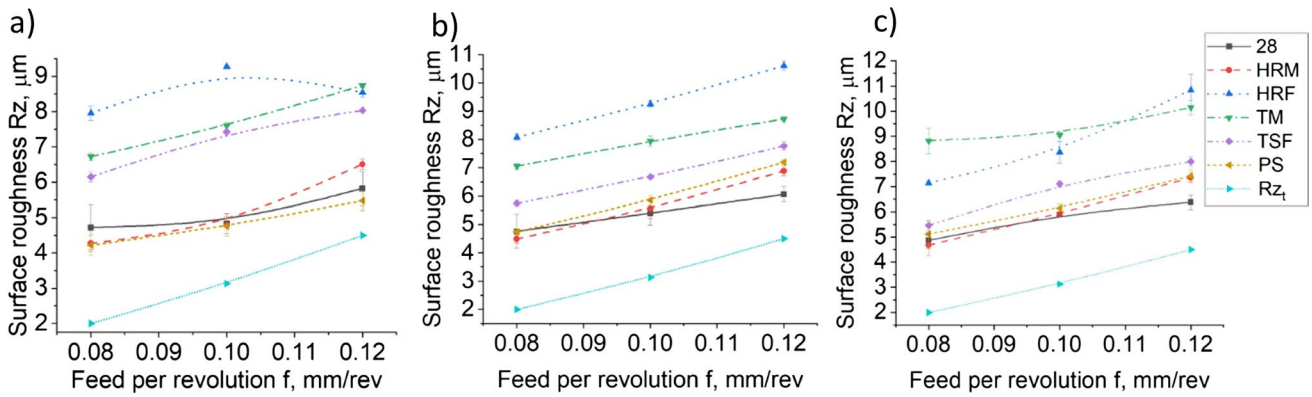
Fig. 13 Surface roughness Rz parameters for different cutting depths: **a** 0.4 mm, **b** 0.8 mm, and **c** 1.2 mm

Table 5 Values of the theoretical Ra_t and Rz_t surface roughness parameter

Feed f, mm	Theoretical Ra_t, µm	Theoretical Rz_t, µm
0.08	0.50	2.00
0.1	0.78	3.13
0.12	1.13	4.50

constant at 0°. In contrast, the negative geometries that produce the lowest roughness possess the smallest radius r_n, approximately 0.02 mm. Although other geometric parameters may vary significantly, the radius r_n emerges as the key parameter that influences surface roughness. Coelho reached similar conclusions, who showed that by changing the radius of the cutting edge, the surface roughness can be significantly influenced [21]. Consequently, the λ and γ angles assume secondary importance, with their influence on surface roughness deemed negligible in the case of negative geometries.

For the lowest feed rate and the smallest depth of cut, the roughness parameter Ra for the HRM geometry was 2.5 times smaller than that for the HRF geometry, with very low dispersion values. As the feed rate and the depth of the cut increased, these differences diminished; however, they remained twice between inserts. Regarding the roughness parameter Rz, the differences between the geometries were smaller, ranging from approximately 100–50% (Fig. 13). Across all sets of cutting parameters, negative geometries 28 and HRM, as well as positive geometry PS, consistently yielded significantly lower roughness values than the other geometries. The results obtained correspond to the work [23], in which it was shown that the best geometry to turn the Inconel 718 alloy is a negative geometry with an effective rake angle of 13° and an edge radius of about 50 µm. However, smaller edge radii have not been tested.

Theoretical values of the parameters Ra_t and Rz_t, derived solely from the kinematics of the turning process, were compared with the real values of the parameters Ra and Rz obtained from experimental tests. It is evident that the real values of the Ra parameter closely resemble that of Ra_t, particularly in the cases of the PS, HRM, and 28 geometries, which exhibit the lowest roughness. On the contrary, the surface roughness generated by other inserts deviates significantly from theoretical values. A surface roughness higher than that theoretically was also observed in the work [13]. This discrepancy between the real and theoretical values of the Rz parameter is probably attributed to the unique mechanical properties of the Inconel 718 alloy. In particular, its substantial ductility and plasticity can lead to material flow during the shaping of roughness profiles, resulting in profile heights that are much higher than those anticipated theoretically. The difference between the real and theoretical roughness may also be due to the occurrence of build-up. Concerning the parameter Ra, the differences between the real and theoretical values escalate with the depth of the cut, possibly due to the increased mechanical load on the tool and the resultant deflection. Greater tool deflection adversely affects the roughness as a result of changes in the effective blade geometry. However, as the feed rate increases and the roughness simultaneously increases, the real values tend to converge towards the theoretical values, as also observed in [36].

Similar to the cutting force components, experimental models were also developed for the roughness parameters Ra and Rz as a function of the cutting parameters. Models were developed separately for selected positive and negative blades that guarantee the lowest surface roughness. Among the negative inserts, geometry 28 provided the lowest roughness, while among the positive inserts, the PS geometry provided the lowest surface roughness for most cutting parameters. The models and their statistical parameters are shown in Table 6, while a graphical representation of the models is provided in Fig. 14.

Table 6 Experimental models of surface roughness parameters

Negative insert VNMG 160404-28					Positive insert VBMT 160,404-PS				
$Ra = -0.143 + 8.30\,f + 0.3308\,a_p$					$Ra = -0.151 + 10.00\,f + 0.2599\,a_p$				
Source	DF	Contr.	F-value	P-value	Source	DF	Contr.	F-value	P-value
Model	2	91.80%	33.59	0.001	Model	2	93.14%	40.75	0.000
Linear	2	91.80%	33.59	0.001	Linear	2	93.14%	40.75	0.000
f	1	56.13%	41.08	0.001	f	1	73.32%	64.16	0.000
a_p	1	35.67%	26.11	0.002	a_p	1	19.83%	17.35	0.006
Error	6	8.20%			Error	6	6.86%		
Total	8	100.00%			Total	8	100.00%		
$Rz = 1.570 + 32.57\,f + 0.734\,a_p$					$Rz = -0.771 + 50.16\,f + 1.768\,a_p$				
Source	DF	Contr.	F-value	P-value	Source	DF	Contr.	F-value	P-value
Model	2	93.34%	42.06	0.000	Model	2	92.08%	34.87	0.000
Linear	2	93.34%	42.06	0.000	Linear	2	92.08%	34.87	0.000
f	1	77.59%	69.93	0.000	f	1	61.51%	46.59	0.000
a_p	1	15.75%	14.20	0.009	a_p	1	30.56%	23.15	0.003
Error	6	6.66%			Error	6	7.92%		
Total	8	100.00%			Total	8	100.00%		

An analysis of the models obtained and the graphical representations of the functions reveals that, in the case of a negative insert, the depth of the cut has a greater influence on the Ra parameter. The contribution of the a_p parameter in the model exceeds 35%. On the contrary, for the PS positive geometry, the contribution of ap is less than 20%. Additionally, in the Rz model for the PS geometry, the parameter ap exhibits an increased *P*-value, indicating its lower statistical significance. Furthermore, when cutting speed and corner radius are included in the model, the contribution of cut depth is so small that it does not appear in the model [28].

In the models of the Rz roughness parameter, the influence of the depth of cut is less pronounced in the negative geometry 28. The contribution of ap in the model of geometry 28 is just under 16%, with the *P*-value of the depth of cut also elevated. Regardless of the type of geometry tested, the forms of the models obtained are similar. The models of the Ra and Rz parameters for geometries 28 and PS differ primarily in the intensity of the influence of feed and depth of cut, as well as their respective values. The PS cutting insert has the geometry that generates the lowest roughness among the tested positive inserts. However, both the Ra and Rz parameters across the entire range of cutting parameters tested yielded higher values for the positive PS geometry than for the negative 28 geometry.

4 Conclusions

By analysing the variability of the cutting force components and basic roughness parameters Ra and Rz of the tested positive and negative insert geometries, it can be concluded that generally, in turning difficult-to-machine alloys such as Inconel, negative inserts are more advantageous, especially those with geometries similar to HRM. The HRM geometry provided the lowest cutting force among almost all the tested cutting parameters, approximately 10% lower than that of the other geometries, particularly with significantly lower active cutting force components. Additionally, while ensuring the lowest cutting force, the HRM geometry produced surfaces with the lowest roughness. This suggests that even in the negative insert configuration of a turning tool, the blade geometry can be shaped to provide the most favourable cutting conditions and the best surface quality for difficult-to-machine alloys such as Inconel after turning. An additional advantage of negative inserts is their double-sided nature, which doubles their cost effectiveness compared to that of positive inserts.

The arrangement of negative inserts in the tool holder enables and simultaneously enforces the application of a negative back rake angle. It has been shown that a negative λ angle causes a slight increase in the radial component F_r, but its value is four times smaller than that of the other components and has a minimal impact on the total cutting force F. Moreover, the largest negative back rake angle λ resulted in the lowest resultant cutting force F and the smallest dispersion of the values of the force components, indicating the highest stability of the cutting process. It has been demonstrated that the best machining effect is achieved when the λ angle is constant along the entire length of the cutting edge. The dominant influence on the feed F_f and tangential F_t cutting force components is the effective rake angle γ, which should remain constant along the cutting-edge length, while the radius of the cutting edge r_n has a secondary effect. Models developed of cutting force
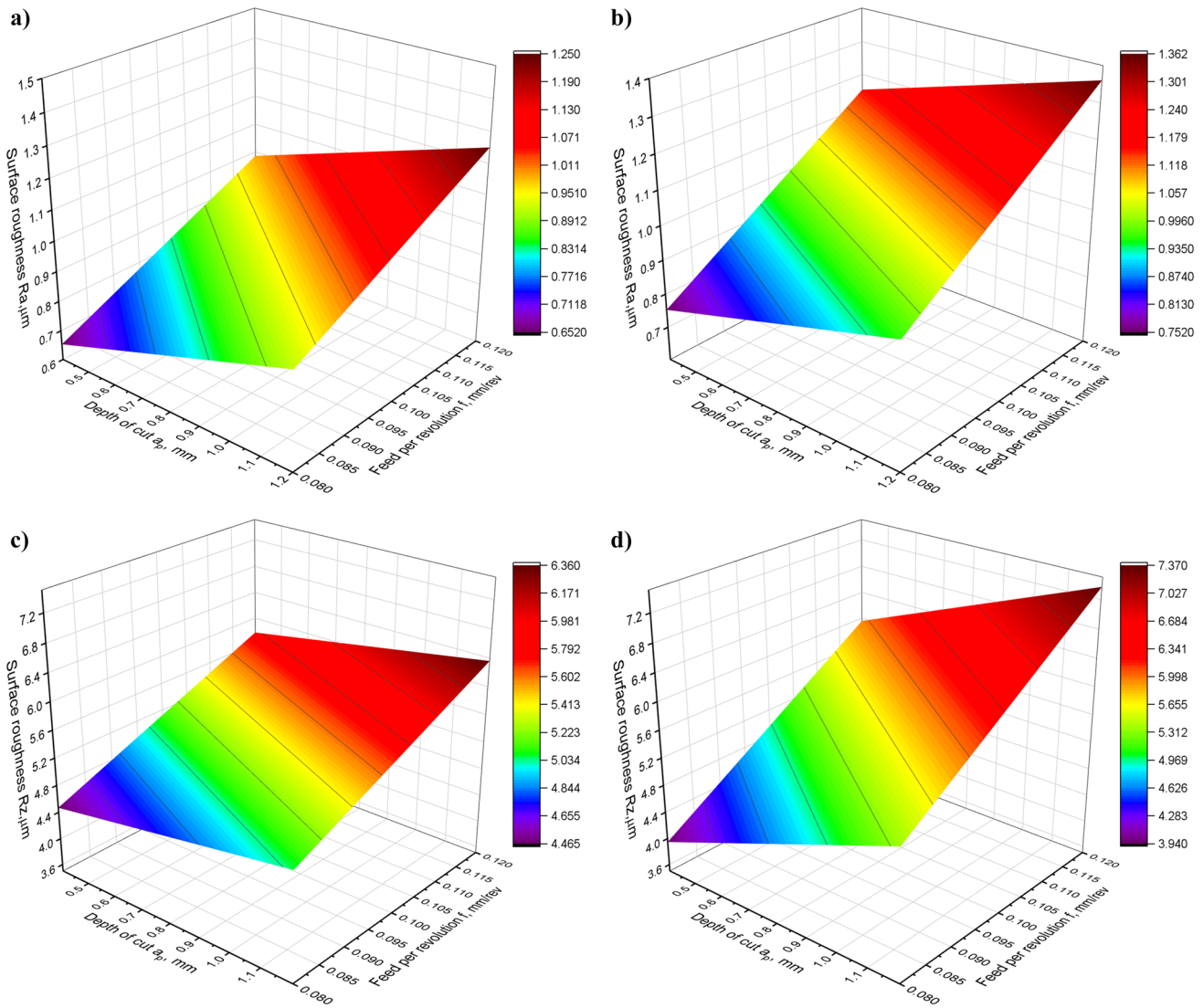
Fig. 14 Graphical representation of models **a** Ra and **c** Rz for 28 geometry, and **b** Ra and **d** Rz for PS geometry

components for selected positive and negative geometries have shown very similar influences of the technological parameters a_p and f on the force values. The main difference between the models of the radial force component F_r lies in the inclination of the negative insert, which results in a negative λ angle.

It has been demonstrated that the radius of the cutting edge r_n is a pivotal parameter that affects the surface roughness. The second most influential factor is the effective rake angle γ. To achieve the lowest surface roughness, it is advisable to employ cutting inserts with the smallest possible radius r_n and the largest positive effective rake angle γ. It has been evidenced that the most favourable geometry for minimising roughness can be achieved on the cutting insert, regardless of whether

it is positive or negative. Additionally, among the examined cutting inserts, the negative geometry yielded the lowest roughness, which may indicate an additional positive effect of a negative lambda angle on surface roughness. Developed models of the Ra and Rz parameters have shown that the impact of technological parameters on surface roughness remains consistent regardless of blade geometry.

The conducted research has demonstrated that utilising positive inserts for machining Inconel alloys with the examined cutting parameters is impractical, primarily due to economic reasons. For negative inserts, an optimal geometry can be defined, ensuring the attainment of the lowest cutting force and surface roughness.

Declarations

Competing interests The authors declare no competing interests.

References

1. Żyłka Ł, Babiarz R (2017) Dressing process in the grinding of aerospace blade root. J Mech Sci Technol 31:4411–4417. https://doi.org/10.1007/s12206-017-0841-6
2. Thakur A, Mohanty A, Gangopadhyay S (2014) Comparative study of surface integrity aspects of Incoloy 825 during machining with uncoated and CVD multilayer coated inserts. Appl Surf Sci 320:829–837. https://doi.org/10.1016/j.apsusc.2014.09.129
3. Roy S, Kumar R, Anurag, et al (2018) A brief review on machining of Inconel 718. Mater Today: Proc 5:18664–18673. https://doi.org/10.1016/j.matpr.2018.06.212
4. Pawade RS, Joshi SS, Brahmankar PK, Rahman M (2007) An investigation of cutting forces and surface damage in high-speed turning of Inconel 718. J Mater Process Technol 192–193:139–146. https://doi.org/10.1016/j.jmatprotec.2007.04.049
5. Lajmert P, Rusinek R, Kruszyński B (2018) Chatter identification in milling of Inconel 625 based on recurrence plot technique and Hilbert vibration decomposition. MATEC Web Conf 148:09003. https://doi.org/10.1051/matecconf/201814809003
6. Buk J, Sułkowicz P, Szeliga D (2023) The review of current and proposed methods of manufacturing Fir tree slots of turbine aero engine discs. Materials 16:5143. https://doi.org/10.3390/ma16145143
7. Jovicic G, Milosevic A, Kanovic Z et al (2023) Optimization of dry turning of Inconel 601 alloy based on surface roughness, tool wear, and material removal rate. Metals 13:1068. https://doi.org/10.3390/met13061068
8. Szablewski P, Legutko S, Mróz A et al (2023) Surface topography description after turning Inconel 718 with a conventional, wiper and special insert made by the SPS technique. Materials 16:949. https://doi.org/10.3390/ma16030949
9. Jeyapandiarajan P, Anthony Xavior M (2019) Influence of cutting condition on machinability aspects of Inconel 718: a review paper. J Engg Res 7:315–332
10. Ramanujam R, Venkatesan K, Saxena V, Joseph P (2014) Modeling and optimization of cutting parameters in Dry turning of Inconel 718 using coated carbide inserts. Procedia Mater Sci 5:2550–2559. https://doi.org/10.1016/j.mspro.2014.07.508
11. Fernández-Lucio P, Pereira Neto O, Gómez-Escudero G et al (2021) Roughing milling with ceramic tools in comparison with sintered carbide on nickel-based alloys. Coatings 11:734. https://doi.org/10.3390/coatings11060734
12. Liu Y, Xu D, Agmell M et al (2021) Numerical and experimental investigation of tool geometry effect on residual stresses in orthogonal machining of Inconel 718. Simul Model Pract Theory 106:102187. https://doi.org/10.1016/j.simpat.2020.102187
13. Zhang B, Njora MJ, Sato Y (2018) High-speed turning of Inconel 718 by using TiAlN- and (Al, Ti) N-coated carbide tools. Int J Adv Manuf Technol 96:2141–2147. https://doi.org/10.1007/s00170-018-1765-8
14. Buddaraju KM, Ravi Kiran Sastry G, Kosaraju S (2021) A review on turning of Inconel alloys. Materials Today: Proceedings 44:2645–2652. https://doi.org/10.1016/j.matpr.2020.12.673
15. Venkatesan K, Ramanujam R, Saxena V et al (2014) Influence of cutting parameters on dry machining of inconel 625 alloy with coated carbide insert - a statistical approach. ARPN J Eng Appl Sci 9:50–258
16. Kacal A (2020) Effect of Machining parameters on turning of Inconel X750 using PVD coated Carbide inserts. https://doi.org/10.56042/jsir.v79i3.68649
17. Zębala W, Słodki B, Struzikiewicz G (2013) Productivity and reliability improvement in turning Inconel 718 alloy – case study. Science and Technology
18. Cantero J, Díaz-Álvarez J, Infante-García D et al (2018) High speed finish turning of Inconel 718 using PCBN tools under dry conditions. Metals 8:192. https://doi.org/10.3390/met8030192
19. Jemielniak K (2009) Rough turning of inconel 718. Adv Manuf Sci Technol 33:5–15
20. Nalbant M, Altın A, Gökkaya H (2007) The effect of cutting speed and cutting tool geometry on machinability properties of nickel-base inconel 718 super alloys. Mater Design 28:1334–1338. https://doi.org/10.1016/j.matdes.2005.12.008
21. Coelho RT, Silva LR, Braghini A, Bezerra AA (2004) Some effects of cutting edge preparation and geometric modifications when turning INCONEL 718™ at high cutting speeds. J Mater Process Technol 148:147–153. https://doi.org/10.1016/j.jmatprotec.2004.02.001
22. Pawade RS, Joshi SS, Brahmankar PK (2008) Effect of machining parameters and cutting edge geometry on surface integrity of high-speed turned Inconel 718. Int J Mach Tools Manuf 48:15–28. https://doi.org/10.1016/j.ijmachtools.2007.08.004
23. Fernández-Valdivielso A, López De Lacalle L, Urbikain G, Rodriguez A (2016) Detecting the key geometrical features and grades of carbide inserts for the turning of nickel-based alloys concerning surface integrity. Proc Inst Mech Eng Part C: J Mech Eng Sci 230:3725–3742. https://doi.org/10.1177/0954406215616145
24. Vetri Velmurgan K, Venkatesan K (2016) An investigation of the parametric effects of cutting parameters on quality characteristics during the dry turning of Inconel 718 alloy. Indian J Sci Technol 9. https://doi.org/10.17485/ijst/2016/v9i44/103314
25. Devillez A, Le Coz G, Dominiak S, Dudzinski D (2011) Dry machining of Inconel 718, workpiece surface integrity. J Mater Process Technol 211:1590–1598. https://doi.org/10.1016/j.jmatprotec.2011.04.011

26. Raykar SJ (2022) Machining performance analysis of turning of Inconel 718 under different coolant environment. https://doi.org/10.56042/ijems.v29i1.46052. IJEMS 29:

27. Kumar S, Singh D, Kalsi NS (2017) Experimental investigations of surface roughness of Inconel 718 under different machining conditions. Mater Today: Proc 4:1179–1185. https://doi.org/10.1016/j.matpr.2017.01.135

28. Frifita W, Ben Salem S, Haddad A, Yallese MA (2020) Optimization of machining parameters in turning of Inconel 718 nickel-base super alloy. Mech Ind 21:203. https://doi.org/10.1051/meca/2020001

29. Yashwant Bhise V, Jogi BF (2022) Effect of cutting speed and feed on surface roughness in dry turning of Inconel X-750. Mater Today: Proc 61:587–592. https://doi.org/10.1016/j.matpr.2022.04.098

30. Mathews M, Nedheesh EB (2014) Modeling and optimisation of cutting and feed forces in turning Inconel 718. Int J Eng Res 3:276–80

31. Reddy MM, William LCS (2020) Finite element analysis: predicting cutting force in turning of Inconel 625 using ceramic tools. IOP Conf Ser: Mater Sci Eng 943:012019. https://doi.org/10.1088/1757-899X/943/1/012019

32. Tebassi H, Yallese MA, Meddour I et al (2017) On the modeling of surface roughness and cutting force when turning of Inconel 718 using artificial neural network and response surface methodology: accuracy and benefit. Period Polytech Mech Eng 61:1–11. https://doi.org/10.3311/PPme.8742

33. Toubhans B, Fromentin G, Viprey F et al (2020) Machinability of inconel 718 during turning: cutting force model considering tool wear, influence on surface integrity. J Mater Process Technol 285:116809. https://doi.org/10.1016/j.jmatprotec.2020.116809

34. Fernández-Abia AI, Barreiro J, Fernández-Larrinoa J et al (2013) Behaviour of PVD coatings in the turning of austenitic stainless steels. Procedia Eng 63:133–141. https://doi.org/10.1016/j.proeng.2013.08.241

35. Yangui H, Zghal B, Kessentini A et al (2010) Influence of cutting and geometrical parameters on the cutting force in milling. ENG 02:751–761. https://doi.org/10.4236/eng.2010.210097

36. Brown I, Schoop J (2020) An iterative size effect model of surface generation in finish machining. JMMP 4:63. https://doi.org/10.3390/jmmp4030063